

***Final Draft***  
**of the original manuscript:**

Golub, M.; Hejazi, M.; Koelsch, A.; Lokstein, H.; Wieland, D.C.F.; Zouni, A.;  
Pieper, J.:

**Solution structure of monomeric and trimeric photosystem I of  
Thermosynechococcus elongatus investigated by small-angle  
X-ray scattering**

In: Photosynthesis Research (2017) Springer

DOI: 10.1007/s11120-017-0342-6

## **Solution structure of monomeric and trimeric Photosystem I of *Thermosynechococcus elongates* by small angle X-ray scattering**

M. Golub<sup>a</sup>, M. Hejazi<sup>b</sup>, A. Koelsch<sup>b</sup>, H. Lokstein<sup>c</sup>, D.C.F. Wieland<sup>d</sup>, A. Zouni<sup>b</sup>, and J. Pieper<sup>a\*</sup>

<sup>a</sup> *Institute of Physics, University of Tartu, Wilhelm Ostwaldi 1, 50411 Tartu, Estonia*

<sup>b</sup> *Humboldt Universität zu Berlin, Philipp Str. 13, 10115 Berlin, Germany*

<sup>c</sup> *Charles University, Faculty of Mathematics and Physics, Department of Chemical Physics and Optics, Ke Karlovu 3, 121 16 Prague, Czech Republic*

<sup>d</sup> *Helmholtz Zentrum Geesthacht, Institute for Materials Research, Department for Metallic Biomaterials, 21502 Geesthacht*

\*Author to whom correspondence should be addressed:

Jörg Pieper  
Institute of Physics, University of Tartu, W. Ostwaldi 1, 50411 Tartu, Estonia.

phone.: + (372) 737 4627

fax: + (372) 738 3033

email: [pieper@ut.ee](mailto:pieper@ut.ee)

Keywords: Photosystem I, n-dodecyl- $\beta$ -D-maltoside, detergent, small angle X-ray scattering,

## Abstract

The structure of monomeric and trimeric photosystem I (PS I) of *Thermosynechococcus elongatus* BP1 (*T. elongatus*) was investigated using small angle X-ray scattering (SAXS). The scattering data reveal that the protein-detergent complexes possess a radius of gyration of 58 and 78 Å in the cases of monomeric and trimeric PS I, respectively. The results also show that the samples are monodisperse, virtually free of aggregation and contain free detergent micelles. The shape of the protein-detergent complexes can be well approximated by elliptical cylinders with heights of 78 Å. Monomeric PS I in buffer solution exhibits minor and major radii of 50 and 85 Å, respectively, while both radii are equal to about 110 Å in the case of trimeric PS I. The data have been analysed using a structure reconstitution by the xyz method. The measurements reveal, that monomeric and trimeric PS I are larger than their respective crystal structures. The reconstituted structures are larger by about 20 Å mainly in the region of the hydrophobic surfaces of the PS I complexes. This contradiction can be resolved by addition of a detergent belt constituted by a single layer of dodecyl- $\beta$ -D-maltoside molecules to the models of monomeric and trimeric PS I, containing 1540 and 480 molecules of the detergent, respectively.

## 1. Introduction

Photosystem I (PS I) is a large membrane-bound pigment-protein supercomplex found in higher plants, algae, and cyanobacteria. It is a light-dependent enzyme that carries out the conversion of solar energy into chemical bond energy. PSI catalysis the light-driven transfer of the electron from the reduced plastocyanin or cytochrome  $c_6$  to oxidized ferredoxin [1]. Electrons from reduced ferredoxin are directly used to reduce required nutrients or are used to produce the more stable biological reductant, NADPH. PSI from the cyanobacterium *Thermosynechococcus elongates* (*T. elongates*) has been crystallised and its structure has been determined to a resolution of 2.5 Å [2]. The monomers of the trimeric PSI core complex (PSIcc) exhibit each 12 protein subunits with 127 cofactors performing light capturing and electron transfer. Nine of them are transmembrane and three are extrinsic subunits at its stromal side. The PsaL subunit forms the interface between these subunits of PS I. The major subunits PsaA and PsaB show an apparent molecular weight of about 83 kDa (each) form a heterodimeric core. They are binding 96 antenna pigment chlorophyll (Chl) a, 22  $\beta$ -carotenoids molecules and further redox cofactors involved in electron-transfer: the primary electron donor P700, a Chl  $a/a'$  dimer; the primary electron acceptor  $A_0$ , a Chl a monomer; the secondary electron acceptor  $A_1$ , a phylloquinone, and ironsulfur [4Fe-4S] clusters. The terminal acceptor molecules represented by two ironsulfur clusters  $F_A$  and  $F_B$  are bound by subunit PsaC, which is one of the three extrinsic subunits located on the stromal side.

PSI is of great interest to biotechnological applications as a photochemical module e.g. to form (??biohybrid electrodes??, other example??) (Stieger et al. 2016a and b, Feifel et al, 2015). The reaction center of trimeric PSI is robust as no light or heat sensitive components have been observed in PSI. Regardless of its wavelength, every absorbed photon generates the charge-separated  $P700^+F_B^-$  state and the thermodynamic efficiency of charge separation is high. In addition, the lifetime of the charge-separated state is long. For biotechnological application some important

informations about the transmembrane core Protein, PSIIc, must be available for a appropriate usage. Next to the type and properties of the used detergent with which PSI has been isolated, the optimal molar concentration of the detergent has to be determined to avoid protein aggregation by low detergent concentrations and to minimize detergent-induced artefacts by too high concentrations. As the detergent can influence the structure and interaction behavior of PSI knowledge about the forming detergent belt of isolated PSI is of strong importance for the later application of this membrane proteins. It has been shown that many of the detergents used for isolation of photosynthetic membrane proteins - e.g. dodecyl- $\beta$ -maltoside ( $\beta$ -DM), heptyl- $\beta$ -thioglucoside (HTG) or octaethylene-glycol-dodecyl-ether (C12E8) - can differently affect the interaction of the proteins in solution. For example, the crystallization of PS II of *T. elongates* was optimized using these different detergents. It led to different resolutions and, interestingly, to a different dehydration behavior of the single samples (Umena et al. 2011, Hellmich et al. 2014).

This raises the questions about the most suitable solubilisation condition, the structure of the detergent molecules surrounding the protein, and about the relevance of the structure determined by crystallographic techniques for solubilised PS I which might deviate under these conditions [3-6]. So far, solubilisation of trimeric PS I has been investigated indirectly by studying the dependence of the PS I fluorescence spectrum on detergent concentration [26]. In this regard, small angle scattering is the experimental techniques of choice to verify shape and size of the PS I-detergent complex directly in solution.

Small-angle neutron and X-ray scattering (SANS and SAXS, respectively) are valuable experimental techniques providing structural information in aqueous environments [19, 20], while neutron spectroscopy probes the dynamics of biomolecules [21, 22]. SANS and SAXS have also been successfully employed in photosynthesis research [23]. For example, neutron studies of plant thylakoid membranes have revealed a size of the grana unit-cell of 157 Å in solution [24, 25], the

hydration dependence of PS II membrane spacing [26], the structural arrangement of cyanobacterial thylakoid membranes [27, 28], but also on state transitions in *Chlamydomonas reinhardtii* [29]. In addition, SANS was also used to characterize the low-resolution structure of the major light-harvesting complex LHC II of green plants [30], PsbO from cyanobacterial photosystem II [31], and the bacterial light-harvesting complex LH2 in solution at physiological temperatures [32].

To understand the functional interaction of the three monomers within the trimer, monomeric PSI from *T. elongatus* has been isolated and characterised (El-Mohsnawy et al. 2011), The monomeric PSI could be isolated as an intact complex with identical antenna size, subunit composition and photochemical activity.

The crystal structure of PS I is shown in Fig. 1. However, the protein is surrounded by a detergent belt which is not visible in the crystal structure due to high thermal mobility of the detergent molecules. As PS I is a transmembrane protein it is necessary to extract it using detergents. Without detergent PS I would not be soluble and aggregate

In the present study, we apply SAXS for structural investigations of monomeric and trimeric PS I of *T. elongatus* under conditions which are typically applied to PS I for crystallization and bio-hybrid electrodes. We determined the radius of gyration, and modelled the structure of monomeric and trimeric PS I containing their respective detergent belt.

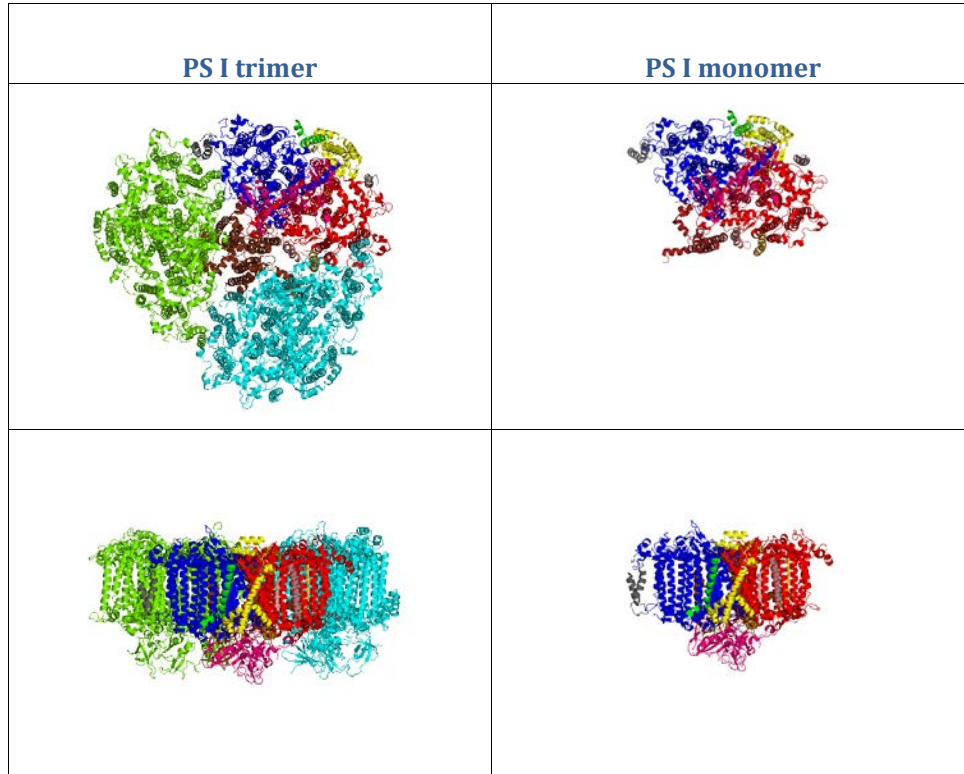


**Figure 1.** The crystal structures of PS I trimer (left) and monomer (right) of *T. elongatus*. Top: view from the luminal side, bottom: view from the membrane plane. The colors represent the different subunits in one monomer and the neighbouring monomers. The figures are adopted from 1JB0 pdb structure, obtained by X-ray diffraction [2].

## 2. Materials and Methods

### Sample Preparation

**Purification of Photosystem I from *T. elongatus*:** Growth conditions of *T. elongatus* BP-1 and extraction of membrane proteins from thylakoids were performed according to Kern et al. [2005]. For the purification of PSI two chromatographic steps were used. The first column was packed with Toyo Pearl DEAE 650 S (Sigma Aldrich) and preequilibrated with buffer A (20 mM MES-NaOH, pH 6.0, 20 mM CaCl<sub>2</sub>, 0.02% β-DM, 5% glycerol). After sample loading and washing the column with buffer A, PSI was separated from PSII using a linear gradient with buffer B (20 mM MES-NaOH, pH 6.0, 20 mM CaCl<sub>2</sub>, 0.02% β-DM, 5% glycerol 100 mM MgSO<sub>4</sub>). PSI containing peak eluted at 80-90 mM MgSO<sub>4</sub> was pooled and diluted with one volume of buffer C (5 mM MES-NaOH, pH 6.0, 0.02 β-DM). The second column was packed with Q-Sepharose™ Fast Flow (GE Healthcare) and preequilibrated with buffer D (5 mM MES-NaOH, pH 6.0, 0.02 % β-DM, 60 mM MgSO<sub>4</sub>). PSI trimer was separated from remaining PSI Monomer by linear gradient with buffer E (5 mM MES-NaOH, pH 6.0, 0.02 % β-DM, 150 mM MgSO<sub>4</sub>). The PSI trimer eluted at 150 mM MgSO<sub>4</sub>. The fractions were pooled and concentrated in an Amicon stirring cell using a Biomax 100 membrane (Millipore). Finally, the PSI Trimer was crystalized by dilution with buffer C at 4 °C until a concentration of 5 mM MgSO<sub>4</sub> was reached. The crystals were collected by centrifugation (5 min, 4°C, 4000 g), washed with buffer C, resolubilized by adding buffer F (5 mM MES-NaOH, pH 6.0, 30 mM MgSO<sub>4</sub>) and recrystalized as described above.

**Assay of PS I activity:** Activity of PSI was measured as oxygen consumption using a Clark-type electrode under saturating light of 1000 μmol photons m<sup>-1</sup> s<sup>-1</sup> at 20 °C. In a final volume of 1 ml, the reaction mixture contained 20 mM Tricine buffer, pH 8.0, 0.2 mg/ml sodium ascorbate, 0.05 mg/ml



methyl viologen, 16  $\mu\text{M}$  cytochrome *c* from horse heart (Sigma-Aldrich) and 0.02 %  $\beta$ -DM. The reaction was started by addition of 5  $\mu\text{g}$  Chlorophyll.

**MS analysis of PS I:** Aliquots (0.5  $\mu\text{l}$  each containing 2  $\mu\text{M}$  PSI) were mixed on the target with 0.5  $\mu\text{l}$  of sinapinic acid matrix solution (dissolved in 40 % (w/v) acetonitrile and 0.1 % (v/v) TFA). The analyte-matrix mixtures were dried under a gentle stream of air. MALDI-TOF mass spectra were recorded on a Bruker Microflex spectrometer (Karlsruhe, Germany) in positive-ion mode. All spectra were measured in linear mode.

**Dynamic light scattering (DLS):** The DLS measurements were performed using a DynaPro NanoStar (Wyatt, USA) with a 787 nm laser. The samples of 6 different protein concentrations ranging from 0.2 to 4.0 mg/ml were filtered prior to use and measured in a disposable 4  $\mu\text{l}$  cuvette (Wyatt, USA). The apparent hydrodynamic radii were approximated to a protein concentration of 0 (infinitely diluted solution) to exclude influences from solution and solute interactions.

#### **Small Angle X-ray Scattering:**

The SAXS experiments on PS I core complexes were carried out using the NanoStar SAXS instrument (Bruker AXS GmbH, Karlsruhe, Germany) [12] at the Helmholtz Zentrum Geesthacht, Germany, where an X-ray beam with a wavelength of 1.54  $\text{\AA}$  is provided by a copper anode. The data were collected by a VANTEC 2000 detector (pixel size 68  $\mu\text{m}$ , active area of 2048x2048 pixels) at a sample-to-detector distance of 103 cm. The samples were placed into glass capillaries with a diameter of 2 mm. The data for each sample were collected in 4 sets of 30 minutes each, to control potential radiation damage of the samples. For each PS I sample three protein concentrations (in the case of trimeric PS I: 10  $\text{mg}\cdot\text{ml}^{-1}$ , 5  $\text{mg}\cdot\text{ml}^{-1}$ , and 2.5  $\text{mg}\cdot\text{ml}^{-1}$ ; in the case of monomeric PS I: 5  $\text{mg}\cdot\text{ml}^{-1}$ , 2.5  $\text{mg}\cdot\text{ml}^{-1}$ , 1  $\text{mg}\cdot\text{ml}^{-1}$ ) have been measured to exclude protein-protein interaction and use the approximation of an infinitely diluted solution. Thus, it was possible to extract

concentration independent SAXS data using the Primus program [13]. The data treatment took into account the scattering from the solvent and capillary, detector efficiency and background signal. The radial averaging of the data was carried out using the Fit2D program [14].

### Data analysis

As the first step, we performed a model independent Guinier analysis. The radius of gyration  $R_g$  was derived from the experimental data according to the classical Guinier approximation:

$$I(q) = I(0) \exp\left(-q^2 \frac{R_g^2}{3}\right), \quad (\text{eq. 1})$$

where  $q$  is the scattering vector,  $I(q)$  is the measured scattering intensity, and  $I(0)$  is the forward scattering, which is a shape independent function of the total scattering power of the sample. The Guinier approximation is valid for small  $q$  values according to  $qR_g \ll 3$  and can be used to determine the size and molecular weight of the scattering objects. If no oligomerization or aggregation is present the scattering cross-section can be approximated for an ideally diluted solution of monodisperse particles by the master formula [15, 16]

$$\frac{d\sigma(q)}{d\Omega(q)} = n\Delta\rho^2 V^2 P(q) S(q), \quad (\text{eq. 2})$$

where  $n$  is the number of particles,  $\Delta\rho$  is the difference in scattering length densities between the particles and the solvent, and  $V$  is the volume of the particles.  $P(q)$  is the form factor, which represents the averaged shape of the scattering particles. The effective structure factor  $S(q)$  is equal to unity for dilute solutions without interaction between the individual particles.

The SAXS data were fitted using a linear superposition of two intensity profiles to mimic a mixture of PSI –  $\beta$ -DM super complexes and free  $\beta$ -DM micelles. The fitting of the SAXS curves was performed using the NSNR SANS software developed at NIST [17].

The form factor of a monodisperse elliptical cylinder used to fit the structure of PS I -  $\beta$ DM super complexes is given by the expression [18]

$$P(q) = \frac{S_{cyl}}{V_{cyl}} \int_0^1 \Psi_{ec} \left( q, a\sqrt{1-x^2} \right) j_0^2 \left( \frac{qLx}{2} \right) dx, \quad (\text{eq. 3})$$

which is normalized by the particle volume  $V_{cyl}$  and averaged over all possible orientations of the elliptical cylinder. Furthermore,  $S_{cyl}$  is a scaling factor,  $a$  is the minor radius of the elliptical cross section,  $L$  is the length of the elliptical cylinder and  $j_0 = \frac{\sin(t)}{t}$  is the zero order Bessel function.

The function  $\Psi_{ec}$  is defined as

$$\Psi_{ec}(q, a) = \frac{1}{\pi} \int_0^\pi \Lambda_1^2 \left[ qa \left( \frac{1+v^2}{2} + \frac{1-v^2}{2} \cos(y) \right)^{1/2} \right] dy, \quad (\text{eq. 4})$$

where  $v$  is the ratio between major radius and minor radius of the elliptical cross section. The function  $\Lambda_1$  is defined as  $\frac{2j_1(t)}{t}$ , where  $j_1 = \frac{\sin(t) - t \cos(t)}{t^2}$  is the first order Bessel function.

The scattering contribution of  $\beta$ DM micelles is taken into account as a spherical core shell, for which the form factor can be written as [19]:

$$P(q) = \frac{S_{sphere}}{V_{sphere}} \left[ \frac{3V_{core}(\rho_{core} - \rho_{shell}) j_1(qr_{core})}{qr_{core}} + \frac{3V_s(\rho_{shell} - \rho_{solv}) j_1(qr_{sphere})}{qr_{sphere}} \right] \quad (\text{eq. 5})$$

where  $S_{sphere}$  is a scale factor,  $V_{sphere}$  is the total volume of the spherical core shell with the radius  $r_{sphere}$ ,  $r_{core}$  is defined as the radius of the core inside the sphere;  $\rho_{shell}$ ,  $\rho_{core}$  and  $\rho_{solv}$  are scattering length densities of the shell, core, and solvent, respectively.

The distance distribution function  $P(r)$  and particle maximum dimension  $D_{\max}$  were determined by fitting the data using the Inverse Fourier transform (IFT) method as implemented in the program GNOM [20]. For the IFT analysis, we have used the limited  $q$ -range up to  $0.1 \text{ \AA}^{-1}$ , where the scattering contribution of  $\beta$ DM micelles can be neglected.

Additionally, the structures of PS I core complexes in solution are obtained using the program DAMMIF, which has been developed by the group of Dmitri Svergun based on a reverse Monte Carlo minimization approach [13, 21]. The final sphere structures were averaged over 20 interactions. To model the PS I trimer, it was taken into account that the trimer is an oblate molecule with  $P3$  symmetry. For the PS I monomer, only the one dimensional limitation of the oblate asymmetry was used. We have also utilized the program CRY SOL [22] in order to calculate a theoretical SAXS curve based on the pdb structure of PS I core complex in monomeric and trimeric forms.

## RESULTS AND DISCUSSION

**Analysis of the protein:** The oligomeric state and purity of monomeric and trimeric PS I were analysed by blue-native PAGE. Both monomeric and trimeric PS I showed a single protein band with high purity and homogeneity (data not shown). The subunit composition of the monomeric and trimeric PSI have been analysed by MALDI-FOF using a linear positive mode. All 12 subunits of PSI known from the 3D crystal structure analysis could be found in the monomeric and trimeric PSI protein samples (supplemental table 1). However, subunits PsaA and B were identified by SDS-PAGE because of their high mass (data not shown). Furthermore, the oxygen consumption rate for both monomeric and trimeric PSI has been calculated to be  $(1670 \pm 70) \mu\text{mol O}_2 \cdot \text{h}^{-1} \cdot \text{mg Chl}^{-1}$  and  $(1860 \pm 150) \mu\text{mol O}_2 \cdot \text{h}^{-1} \cdot \text{mg Chl}^{-1}$ , respectively.

**Model independent analysis:** SAXS data of monomeric and trimeric PS I are shown in the left panel of Fig. 2. Guinier plots of the same data sets are displayed in the right panel of Fig. 2 for  $q^2$ -values up to  $0.09 \text{ \AA}^{-2}$ . The widely linear dependence of  $\text{Ln}[I(q)]$  on  $q^2$  in the Guinier region (see right panel of Fig. 2) indicates that both samples are monodisperse and virtually free of aggregation/protein-protein interactions at the given concentrations, which was confirmed by dynamic light scattering (DLS).

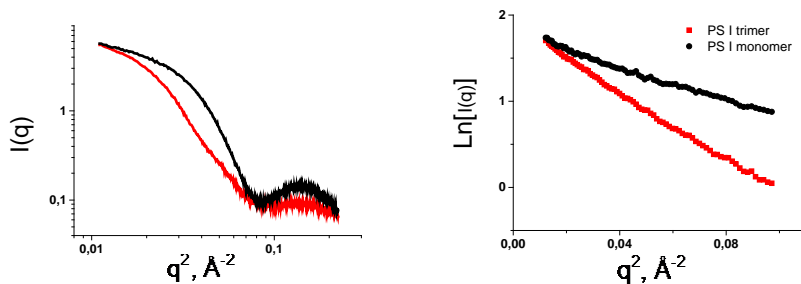


**Figure 2.** SAXS curves of solubilized PS I in monomeric (black) and trimeric form (red). The left panel shows the full  $q$ -range in log/log scale, the right panel presents the Guinier plots at small  $q$  values.

**Please check the x-axis of Figure 2 and 3: identical curves, but in Fig2 it is  $q^2$  and Fig3  $q$ . Also we can't see the  $1.4 \text{ \AA}^{-1}$  in the axis.**

The radius of gyration  $R_g$  can be determined according to Eq. 1 by doing a linear regression of the Guinier plot shown in Fig. 2. The  $R_g$  value obtained for the PS I monomer is equal to about  $58 \text{ \AA}$ , which is  $10 \text{ \AA}$  larger than the  $R_g$  value calculated from the known crystal structure structure [2]. This deviation can be attributed to the presence of a detergent belt around the PS I monomer, see also discussion below. The respective  $R_g$  value for the PS I trimer is about  $78 \text{ \AA}$ .

#### DLS Analysis

The hydrodynamic radii ( $R_H$ ) of monomeric and trimeric PS I was measured by DLS at 6 different concentrations and approximated to a concentration of 0. The  $R_H$  for both proteins was  $69 \text{ \AA}$  and  $98 \text{ \AA}$ , respectively. The ratio  $R_g/R_H$  was 0.84 and 0.80 for monomeric and trimeric PS I, respectively. These values are higher than the values of a spherical shape (0.77). This deviation can be accounted to the ellipsoidal shape of the proteins.

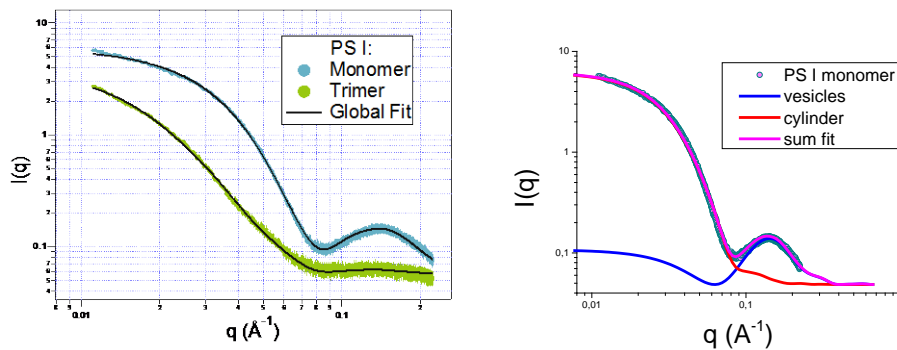


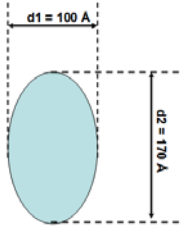
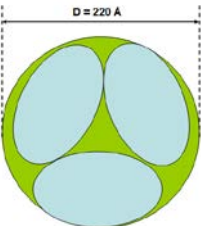
**Figure 3.** Analysis of the SAXS data by the combined model of an elliptical cylinder representing the PS I-detergent complex and a core shell sphere representing free micelles according to Eq. XX. Left panel: global fit (black lines) of SAXS data of monomeric (blue) and trimeric PS I (green), see Table 1 for parameters. The SAXS curves are rescaled for ease of inspection. Right panel: individual contributions to the combined fit (violet line) of SAXS data of monomeric PS I (blue). The elliptical cylinder representing the PS I-detergent supercomplex is shown as a red line, the spherical vesicles by a blue line.

**Model-based analysis:** Both, the SAXS curves of monomeric and trimeric PS I, reveal a distinct peak around a  $q$ -value of about  $0.14 \text{ \AA}^{-1}$  (Fig. 2) please check the number and the x-axis. Such a peak is not expected from the protein-detergent complex itself, since it indicates the presence of a relatively small structure with an average size of about  $35\text{-}40 \text{ \AA}$ , i.e. it is smaller than the  $R_g$ -values of the PS I complexes determined above. The additional peak can most probably be attributed to free micelles. As the so far performed analysis gives only some information on the size of PSI but not on the structure simple geometrical shapes were fitted to the data. Here PSI can be best described by elliptical cylinder due to its asymmetric and complex structure, see Fig.1- It has to be kept in mind, however, that SAXS cannot distinguish the PS I complex and free detergent. Thus, the SAXS curves were fitted by a superposition of an elliptical cylinder, which corresponds to the protein-detergent complex, and a spherical core shell, which was applied to take into account the contribution of free  $\beta$ -DM micelles (Fig. 3B). In order to decrease the number of free variables, a global fit was carried

out, where the parameters of the free vesicles and the lengths of the elliptical cylinders were set to be the same for the SAXS data of monomeric and trimeric PS I, respectively. In terms of structural parameters of PS I, only the minor and major radii of the elliptical cylinder were treated as free parameters. As shown in Fig. 3, the fits achieved using this model show a very good agreement with the SAXS data of monomeric and trimeric PS I, respectively. The two individual contributions resulting from PS I and free micelles are plotted in the right panel of Fig. 3. Table 1 summarized the complete set of fit parameters and sketches of the elliptical cross sections in monomeric and trimeric PS I. Here, the minor and major radii of the elliptical cylinder approximately represent the smallest and largest dimensions of the PS I-detergent complex (cf. the upper panels of Fig. 1 for the PS I contribution), while the length of the cylinder is close to the height of PS I membrane intrinsic and extrinsic components (cf. the lower panels of Fig. 1 for the lateral view of PS I). Sketches on the basis of the extracted parameters of the elliptical cross sections found for monomeric and trimeric PS I, respectively, are shown in Table 1. The sketches also reveal that three elliptical cross sections as determined for monomeric PS I fit into the cross section found for trimeric PS I. The parameters of the free vesicles are in a good agreement with the known values for the detergent  $\beta$ -DM, which self organizes in spherical micelles, the radius of which is about 37.4 Å above the critical micelle concentration [23, 24]. Our analysis shows that at  $q$  smaller than 0.1 Å<sup>-1</sup> the scattering from PS I complexes is two orders of magnitude higher than the scattering of the micelles and, thus, dominates the scattering signal (Figure 3B). Following this, the scattering contribution from the  $\beta$ -DM micelles can be neglected in the region of small  $q$ -values.

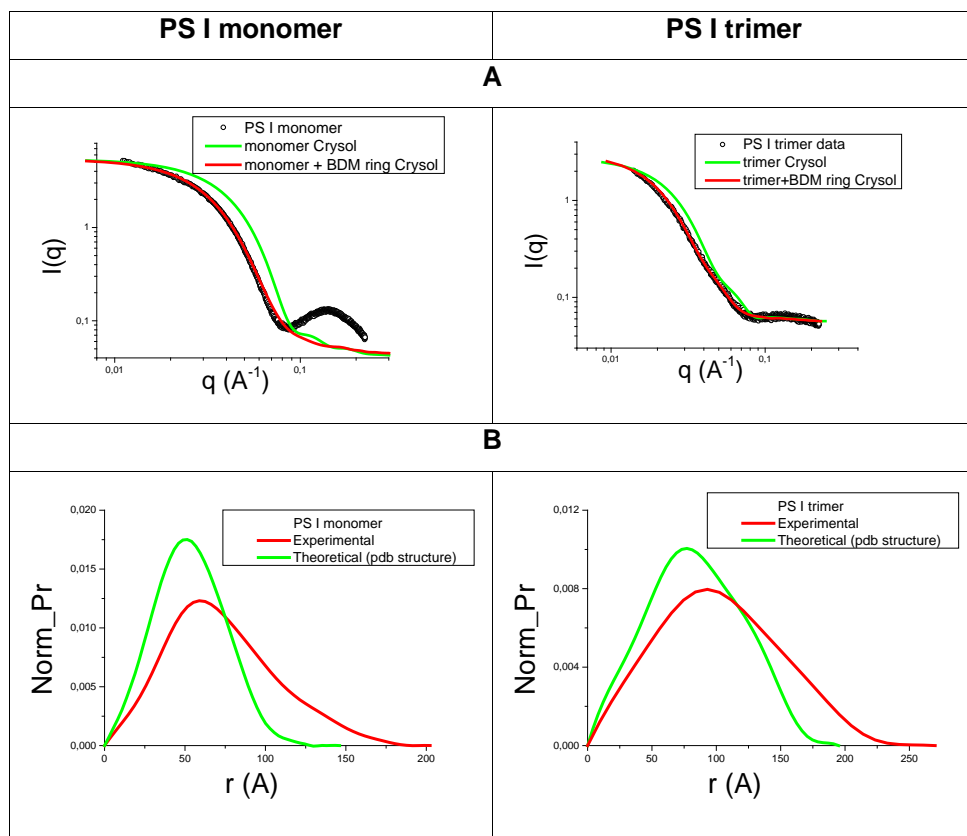


Table 1. Radii of monomeric and trimeric PS I as fitted from Fig. 3.

PS I protein	Monomer	Trimer
Top view		
<b>Elliptical cylinder scale</b>	0.03	0.005
minor radius $d1/2$ (Å)	<b>50±5</b>	<b>110±5</b> (19% polydispersity)
major radius $d2/2$ (Å)	<b>85±5</b>	<b>110±5</b>
length (Å)	71±5	71±5
SLD cylinder (Å <sup>-2</sup> )	8 e-06	8 e-06
SLD solvent (Å <sup>-2</sup> )	9.46 e-06	9.46 e-06
<b>Spherical vesicles scale</b>	3.9	0.22
core radius (Å)	10.9	10.9
shell thickness (Å)	26.5	26.5
Core SLD (Å <sup>-2</sup> )	8.1 e-06	8.1e-06
Shell SLD (Å <sup>-2</sup> )	9.52 e-06	9.5 e-06
Solvent SLD (Å <sup>-2</sup> )	9.46 e-06	9.46 e-06
bkg (cm <sup>-1</sup> )	0.05	0.056

**Modelling of the detergent belt around PS I:** For further analysis, it was verified whether the crystal structures of the PS I monomer and trimer reproduce the respective experimental SAXS data. The CRY SOL program was applied to calculate the model SAXS curves from the known pdb structures [refs.]. As shown in Fig. 4A the SAXS curves simulated based on the crystal structures of PS I do not completely reproduce the experimental data sets. Rather, the crystal structures appear to correspond to smaller structures as they are shifted to higher q-values. Most likely, the reason for this deviation is the presence of a  $\beta$ -DM detergent belt around PS I, which increases the apparent size of the molecule.

The presence of  $\beta$ -DM detergent belts for both, monomeric and trimeric PS I, is also visible in the shapes of the pair distribution functions  $P(r)$ . Fig. 4B shows the  $P(r)$  function calculated by an indirect Fourier transformation (IFT) using GNOM from i) the experimental SAXS data (red lines) and ii) the X-ray crystal structures of monomeric and trimeric PS I (green lines). The  $P(r)$  functions calculated from the experimental SAXS data exhibit peak positions at about 60 Å in case of the PS I monomer and at about 93 Å in case of the PS I trimer (Fig. 4B). The latter values are approximately 10 Å larger than the theoretically expected values (see green curves in Fig. 4B).



**Figure 4.** PS I SAXS data in comparison to the crystal structure:

Panel A): Experimental SAXS curves (black dots) with fits based on the corresponding PS I crystal structures only (green lines) and assuming a detergent belt around PS I (red lines).

Panel B): Normalized  $P(r)$  functions of PS I monomer (left) and PS I trimer (right) derived from the experimental SAXS data (red lines) and from the PS I X-ray crystal structures (green lines) by inverse Fourier transform.

Panel A): Experimental SAXS curves (black dots) with fits based on the crystal structure of PS I only (green) and assuming a detergent belt around PS I (red)

Panel B: Normalized size distribution ( $P(r)$ ) functions derived from the experimental SAXS data (color) and from the PS I crystal structures (color) by inverse Fourier transform.

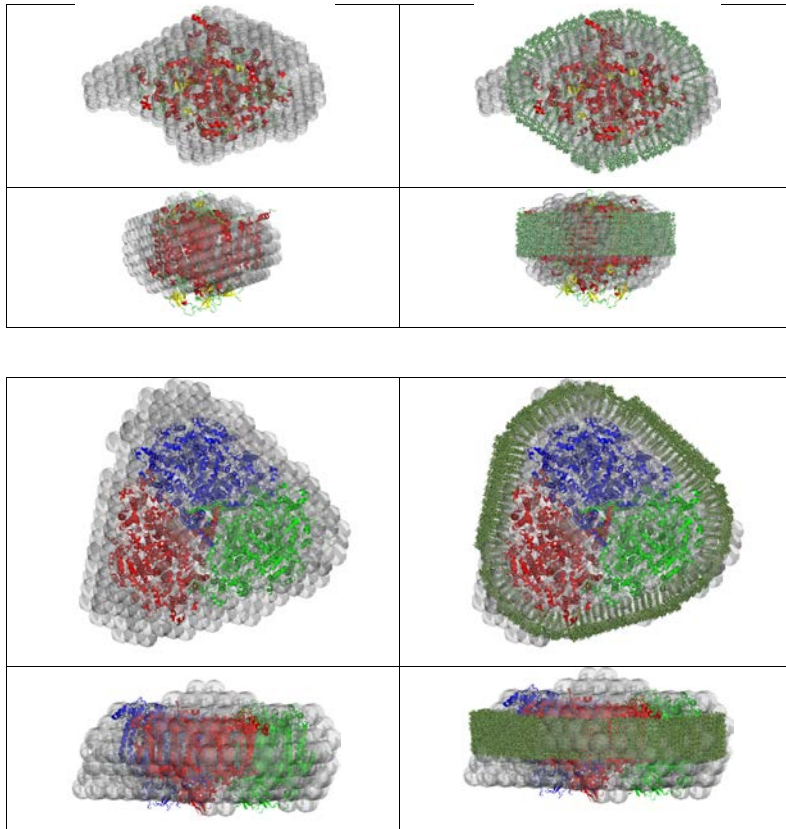


**Figure 6.** Structure reconstitution of the PS I trimer. The top view is shown in the upper line, the lateral view in the lower line. The left column shows the structure reconstitution (grey spheres) based on Monte Carlo simulations, the right column depicts PS I and an additional detergent belt of  $\beta$ -DM molecules (green).

Structure reconstitutions of PS I monomers and trimers based on Monte Carlo simulations from the  $P(r)$  functions obtained above are shown by grey spheres in the left panels of Fig. 5 and Fig. 6, respectively, and compared to the corresponding crystal structures. As already suggested by the experimentally obtained  $P(r)$  functions (Fig. 4), the PS I- $\beta$ -DM complexes under study are larger than expected from the crystal structures. Especially, it is apparent from Fig. 5 and 6, that the additional structures surrounding the PS I molecules are mainly visible in the top views, while the lateral dimension is reproduced rather well. Therefore, the reconstituted structures suggest the presence of a detergent belt with a thickness of about 20 Å attached to the hydrophobic surfaces of PS I protein. This interpretation is in good agreement with previous investigations on membrane protein-detergent interactions, which revealed a monolayer ring of detergent molecules bound to membrane proteins in general [3, 23, 25]. In the case of trimeric PS I in  $\beta$ -DM, a 27 Å broad detergent monolayer was also deduced from the dependence of the PS Icc fluorescence spectrum on the detergent concentration [26].

Therefore, the initial crystal structures of PS I monomer and trimer were embedded in monolayer belts of  $\beta$ -DM molecules that surrounds the hydrophobic part of the proteins (right panels of Figs. 5 and 6).

Why is there only 1/3<sup>rd</sup> of the DDM around the Monomer compared to the trimer? If I assume the belt to be a circle, the trimer has a circumference of  $2\pi r$ , while one monomer would be  $\frac{1}{3}(2\pi r)$ . So the circumference should be around  $\frac{1}{3}(2\pi r) + 2r$  instead of  $\frac{1}{3}(2\pi r)$  and therefore 1/3<sup>rd</sup> of belt-volume does not seem logical to me. Was there a number mixed up?

It is apparent that the resulting PS I- $\beta$ -DM complex almost perfectly accounts for the structure reconstructed from the SAXS data. Based on the latter model, it is possible to estimate the number of  $\beta$ -DM molecules in the PS I-detergent complex to be about 480 in the case of the PS I monomer

and about 1540  $\beta$ -DM molecules in the case of the PS I trimer. The latter value is in good agreement with the 1160 molecules obtained by Müh and Zouni [26]. Yet it is twice as large as the 800 molecules obtained by SANS (Le et al. 2014). In summary, it can be concluded that it is possible to measure the detergent belt around membrane proteins by SAXS. We revealed the structures of PS I monomer and trimer in conditions which are typically applied to photosystems in crystallization and biotechnological applications.. The data directly prove the detergent belts to be constituted by a monolayer of  $\beta$ -DM molecules around the hydrophobic transmembrane areas.

## Acknowledgements

Financial Support by the Estonian Science Foundation (Grant No. 9453) and the Estonian Research Council (Grant IUT02-28) is gratefully acknowledged. J. P. is also deeply indebted to the European Social Fund's Internationalisation Programme DoRa for financial support. H.L. acknowledges GAČR grant No. P501/12/G005. We thank Dr. Joerg Fettke, University of Potsdam (Germany) for kindly giving access to the Bruker Microflex spectrometer.

Supplemental table 1: MALDI-TOF analysis of subunit composition of trimeric and monomeric PSI.

	PsaM	PsaX	PsaI	PsaJ	PsaE	PsaK	PsaC	PsaF	PsaD	PsaL
<b>Calculated mass* (Da)</b>	<b>3424</b>	<b>4101</b>	<b>4166</b>	<b>4767</b>	<b>8389</b>	<b>8480</b>	<b>8800</b>	<b>15113</b>	<b>15370</b>	<b>16251</b>
<b>Monomer</b>	3423	3970	4191	4796	8262	8393	8674	15126	15228	16145
<b>Trimer</b>	3423	3970	4195	4797	8263	8394	8674	15122	15235	16132

\*post translational modification of PS I subunits are described in detail (El-Mohsnawy et al. 2010)

## References

New:

J. Kern, B. Loll, C. Lüneberg, D. DiFiore, J. Biesiadka, K.-D. Irrgang, and A. Zouni, (2005) *Biochim. Biophys. Acta*, 1706, 147–157.

1. Golbeck, J.H., *Structure, function and organization of the Photosystem I reaction center complex*. *Biochim Biophys Acta*, 1987. **895**(3): p. 167-204.
2. Liu, Z.F., et al., *Crystal structure of spinach major light-harvesting complex at 2.72 angstrom resolution*. *Nature*, 2004. **428**(6980): p. 287-292.
3. le Maire, M., P. Champeil, and J.V. Moller, *Interaction of membrane proteins and lipids with solubilizing detergents*. *Biochim Biophys Acta*, 2000. **1508**(1-2): p. 86-111.
4. Seddon, A.M., P. Curnow, and P.J. Booth, *Membrane proteins, lipids and detergents: not just a soap opera*. *Biochimica Et Biophysica Acta-Biomembranes*, 2004. **1666**(1-2): p. 105-117.
5. Mo, Y., et al., *Detergent-Associated Solution Conformations of Helical and beta-Barrel Membrane Proteins*. *Journal of Physical Chemistry B*, 2008. **112**(42): p. 13349-13354.
6. Cardoso, M.B., et al., *Insight into the Structure of Light-Harvesting Complex II and Its Stabilization in Detergent Solution*. *Journal of Physical Chemistry B*, 2009. **113**(51): p. 16377-16383.
7. Zouni, A., et al., *Crystal structure of photosystem II from *Synechococcus elongatus* at 3.8 Å resolution*. *Nature*, 2001. **409**(6821): p. 739-43.
8. Neylon, C., *Small angle neutron and X-ray scattering in structural biology: recent examples from the literature*. *European Biophysics Journal with Biophysics Letters*, 2008. **37**(5): p. 531-541.
9. Petoukhov, M.V. and D.I. Svergun, *Joint use of small-angle X-ray and neutron scattering to study biological macromolecules in solution*. *European Biophysics Journal with Biophysics Letters*, 2006. **35**(7): p. 567-576.
10. Petoukhov, M.V. and D.I. Svergun, *Analysis of X-ray and neutron scattering from biomacromolecular solutions*. *Current Opinion in Structural Biology*, 2007. **17**(5): p. 562-571.
11. Trehwella, J., *Neutrons reveal how nature uses structural themes and variation in biological regulation*. *Physica B-Condensed Matter*, 2006. **385-86**: p. 825-830.
12. *NanoStar*. 2015; Available from: <https://www.bruker.com/products/x-ray-diffraction-and-elemental-analysis/x-ray-diffraction/nanostar/overview.html>.
13. Konarev, P.V., et al., *PRIMUS: a Windows PC-based system for small-angle scattering data analysis*. *Journal of Applied Crystallography*, 2003. **36**: p. 1277-1282.
14. Hammersley, A.P., et al., *Two-Dimensional Detector Software: from Real Detector to Idealised Image of Two-Theta Scan*. *High Pressure Research*, 1996. **14**: p. 235-248.
15. Kikhney, A.G. and D.I. Svergun, *A practical guide to small angle X-ray scattering (SAXS) of flexible and intrinsically disordered proteins*. *FEBS Lett*, 2015. **589**(19 Pt A): p. 2570-7.
16. Jacques, D.A. and J. Trehwella, *Small-angle scattering for structural biology--expanding the frontier while avoiding the pitfalls*. *Protein Sci*, 2010. **19**(4): p. 642-57.
17. Kline, S.R., *Reduction and Analysis of SANS and USANS Data Using IGOR Pro*. *Journal of Applied Crystallography*, 2006. **39**: p. 895-900.
18. Feigin, L.A. and D.I. Svergun, *Structure Analysis by Small-Angle X-Ray and Neutron Scattering*, G.W. Taylor, Editor. 1987, Plenum Press: New York.
19. Guinier, A. and G. Fournet, *Small-Angle Scattering of X-Rays*. 1955, New York: John Wiley and Sons.
20. Svergun, D.I., *Determination of the Regularization Parameter in Indirect-Transform Methods Using Perceptual Criteria*. *Journal of Applied Crystallography*, 1992. **25**: p. 495-503.
21. Franke, D. and D.I. Svergun, *DAMMIF, a program for rapid ab-initio shape determination in small-angle scattering*. *Journal of Applied Crystallography*, 2009. **42**: p. 342-346.
22. Svergun, D.I., C. Barberato, and M.H.J. Koch, *CRY SOL -a Program to Evaluate X-ray Solution Scattering of Biological Macromolecules from Atomic Coordinates*. *J. Appl. Cryst.*, 1995. **28**: p. 768-773.

23. Moller, J.V. and M. le Maire, *Detergent binding as a measure of hydrophobic surface area of integral membrane proteins*. J Biol Chem, 1993. **268**(25): p. 18659-72.
24. Neugebauer, J.M., *Detergents: an overview*. Methods Enzymol, 1990. **182**: p. 239-53.
25. Pebay-Peyroula, E., et al., Detergent structure in tetragonal crystals of OmpF porin. Structure, 1995. **3**(10): p. 1051-9.
26. Müh, F. and A. Zouni, Micelle formation in the presence of photosystem I. Biochim Biophys Acta, 2008. **1778**(10): p. 2298-307.

Le, R.K. et al. *Analysis of the solution structure of Thermosynechococcus elongates photosystem I in n-dodecyl-b-D-maltoside using small-angle neutron scattering and molecular dynamics simulation*. Archives of Biochemistry and Biophysics, 2014. **550-551**: p. 50–57.

Stieger, K.R. et al. *Engineering of supramolecular photoactive protein architectures: the defined co-assembly of photosystem I and cytochrome c using a nanoscaled DNA-matrix*. Nanoscale, 2016. **8**: p. 10695-10705.

Mukherjee et al. *Detergent–protein interactions in aqueous buffer suspensions of Photosystem I (PS I)*, 2011. **358**: p. 477–484.

El-Mohsnawy E. et al. Structure and Function of Intact Photosystem 1 Monomers from the Cyanobacterium Thermosynechococcus elongates, Biochemistry, 2010, 49: p. 4740-4751.

Watanabe M. et al. Novel Supercomplex Organization of Photosystem I in Anabaena and Cyanophora paradoxa, 2011, 52: p. 162-168.

Umena Y et al. Crystal structure of oxygen-evolving photosystem II at a resolution of 1.9 Å, Nature, 2011, **473**: p. 55-60

Stieger, K.R., Feifel, S.C., Lokstein, H., Hejazi, M., Zouni, A., and Lisdat, F. (2016). Biohybrid architectures for efficient light-to-current conversion based on photosystem I within scalable 3D mesoporous electrodes. Submitted

Stieger, K.R., Ciornii, D., Kölsch, A., Hejazi, M., Lokstein, H., Feifel, S.C., Zouni, A., and Lisdat, F. (2016). Engineering of supramolecular photoactive protein architectures: Defined co-assembly of photosystem I and cytochrome c using a nanoscaled DNA-matrix. *Nanoscale* **8**, 10695-10705.

Feifel, S.C., Lokstein, H., Hejazi, M., Zouni, A., and Lisdat, F. (2015). Unidirectional photocurrent of photosystem I on  $\pi$ -system-modified graphene electrodes: nanobionic approaches for the construction of photobiohybrid systems. *Langmuir* **31**, 10590–10598.

27. Kern, J., et al., Purification, characterisation and crystallisation of photosystem II from Thermosynechococcus elongatus cultivated in a new type of photobioreactor. Biochim Biophys Acta, 2005. 147-157